

Influence of chirp, jitter and relaxation oscillations on probabilistic properties of laser pulse interference

Roman Shakhovoy, Violetta Sharoglazova, Alexander Udaltsov, Alexander Duplinskiy, Vladimir Kurochkin, and Yury Kurochkin

Abstract—The study of laser pulse interference in the context of quantum technologies, particularly, concerning its probabilistic properties in quantum random number generators and in quantum key distribution systems, gains new relevance today. Here, we consider in detail the influence of chirp, jitter and relaxation oscillations on the probability density function of the interference of gain-switched semiconductor laser pulses. It is shown how to reduce the combined impact of chirp and jitter using a telecom bandpass filter. Experimental results are reproduced by Monte-Carlo simulations using a rigorous model based on the solution of laser rate equations.

Index Terms—Interference, chirp, jitter, optical pulses, semiconductor lasers.

I. INTRODUCTION

LASER pulse interference is an essential ingredient of quantum technologies. Weak coherent states (attenuated laser pulses) are widely used to mimic interference between single photons, which is generally employed in such quantum information applications as quantum teleportation [1], linear optics computing [2] and detector-safe quantum cryptography [3], [4]. Interference of intense coherent states, in turn, is often used in optical quantum random number generators (QRNGs) [5]–[9], where phase randomness between pulses of a gain-switched laser acts as a source of quantum entropy. In both “single-” and multi-photon cases, the interference of laser pulses often has a number of unpleasant features, which adversely affect the visibility of the interference and have an impact on the appearance of the probability density function (PDF) of the random interference signal. The study of laser pulse interference in the context of quantum technologies, particularly, concerning its probabilistic properties in QRNGs and in quantum key distribution systems, gains new relevance today.

The most crucial features of laser pulse interference are inevitable chirping of laser frequency under direct modulation and fluctuations of the pulse emission time (jitter). These effects are particularly noticeable in standard telecom lasers, which are usually not well suited for interferometric applications. The combined influence of these two effects in the context of QRNG was considered in [7], where authors demonstrated that the PDF of the interference signal for chirped laser pulses differs markedly from the PDF measured in the absence of chirp. The authors proposed a simple model, in which laser pulses were assumed to have a Gaussian shape and exhibit a linear chirp. The main disadvantage of their model was an assumption of uniform PDF for the jitter needed to fit theoretical results to experimental data. However, distribution of pulse emission time fluctuations can be shown to be quite close to Gaussian in case of gain-switched lasers [10] and usually has the rms of the order of 10-50 ps [11], [12]. More detailed investigation reveals that the appearance of the interference signal PDF with more realistic jitter is different from the one observed in [7], so the laser pulse interference model should be refined and expanded.

In the present work, we use a more rigorous model, which considers relaxation oscillations in addition to jitter and chirp. The combined influence of all three effects is considered by solving laser rate equations. Such an approach allows describing the interference of laser pulses distorted by relaxation oscillations and helps explaining the change of the PDF of the interference signal after cutting off the high-frequency part of the laser spectrum with optical bandpass filter.

II. THEORY

Let us first consider the laser pulse interference measured using a Michelson fiber optic interferometer (Fig. 1). The delay line ΔL is chosen so that the corresponding delay time defined by $\Delta T = 2\Delta L n_g / c$ is multiple of the pulse repetition period $2\pi/\omega_p$, such that at the output of the interferometer the i -th laser pulse of the sequence meets the $i + N_p$ -th pulse, where N_p is the number of pulses that pass the short arm during the time needed for the pulse to pass the long arm (here c is the light speed in vacuum and n_g is the group index).

R. Shakhovoy, A. Udaltsov, A. Duplinskiy, and V. Kurochkin are with Russian Quantum Center, 121205 Moscow, Russia, and also with QRate, 121353 Moscow, Russia (e-mail: r.shakhovoy@gograte.com).

V. Sharoglazova is with Russian Quantum Center, 121205 Moscow, Russia, QRate, 121353 Moscow, Russia, and also with Skolkovo Institute of Science and Technology, 121205 Moscow, Russia.

Y. Kurochkin is with Russian Quantum Center, 121205 Moscow, Russia, QRate, 121353 Moscow, Russia, and also with NTI Center for Quantum Communications, National University of Science and Technology MISiS, 119049 Moscow, Russia.

In the following, subscripts 1 and 2 will be used to designate the short and long arms of the interferometer, respectively, and to designate laser pulses coming from the respective arms. Assuming that interfering pulses are polarized in the same plane, the intensity of the signal at the output of the interferometer can be written as follows:

$$S(t) \sim |E_1(t) + E_2(t)|^2, \quad (1)$$

where E_1 and E_2 are (scalar) electric fields in the first and second pulses, respectively. The time dependence of the electric field in a pulse can be written in the following form:

$$E_{1,2}(t) \sim \sqrt{P_{1,2}(t)} e^{i\varphi_{1,2}(t)}, \quad (2)$$

where $\varphi_{1,2}(t)$ is the phase of the field and $P_{1,2}(t)$ is the output power in the corresponding pulse. The power of the interfering pulses can be related to the laser output power $P(t)$ as follows:

$$\begin{aligned} P_1(t) &= (1 - a_1) T_{01} T_{10} P(t), \\ P_2(t) &= (1 - a_2) T_{02} T_{20} P(t - \Delta t), \end{aligned} \quad (3)$$

where a_1 and a_2 stand for the losses in the optical fiber in the short and long arms, respectively, T_{kl} is a coupler transmittance from the input port k to the output port l (see Fig. 1), and where we introduced the inaccuracy of the pulse overlap Δt , i.e. we took into account that one of the pulses may exit the interferometer a bit earlier than the other.

Time evolution of the power P and the phase φ of the electric field in the laser pulse can be found from the system of standard laser rate equations [13]–[16]:

$$\begin{aligned} \frac{dQ}{dt} &= (G - 1) \frac{Q}{\tau_{ph}} + C_{sp} \frac{N}{\tau_e}, \\ \frac{d\varphi}{dt} &= \frac{\alpha}{2\tau_{ph}} (G_L - 1), \\ \frac{dN}{dt} &= \frac{I}{e} - \frac{N}{\tau_e} - \frac{QG}{\Gamma\tau_{ph}}. \end{aligned} \quad (4)$$

Here Q is the absolute square of the normalized electric field amplitude corresponding to the photon number inside the laser cavity and related to the output power by $P = Q(\varepsilon\hbar\omega_0/2\Gamma\tau_{ph})$, where $\hbar\omega_0$ is the photon energy (ω_0 is the carrier frequency), ε is the differential quantum output, Γ is the confinement factor, τ_{ph} is the photon lifetime inside the cavity, and the factor $1/2$ takes into account the fact that the output power is generally measured from only one facet. Onwards, N is the carrier number, I is the pump current, e is the absolute value of the electron charge, τ_e is the effective lifetime of the electron, the factor C_{sp} corresponds to the fraction of spontaneously emitted photons that end up in the active mode, α is the linewidth enhancement factor (Henry factor [17]), and the dimensionless linear gain G_L is defined by

$G_L = (N - N_0)/(N_{th} - N_0)$, where N_0 and N_{th} are the carrier numbers at transparency and threshold, respectively. The gain saturation [15] is included in Eq. (4) by using the relation $G = G_L(1 - \chi P)$, where χ is the gain compression factor [13].

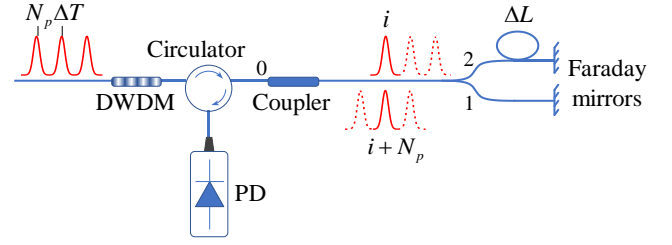


Fig 1. The optical scheme used in this work to observe interference of laser pulses. The circulator is used to separate optical signals that travel in opposite directions and thus to prevent unwanted feedback into a laser. PD stands for the photodetector; DWDM – dense wavelength division multiplexing bandpass filter. ΔT and ΔL are defined in the text.

The signal corresponding to a pair of interfering pulses can be now written in the following form:

$$\begin{aligned} S(t) &\sim \left| \sqrt{P_1(t)} \exp[i\varphi(t) + i\varphi_{p1} + i\theta_1] \right. \\ &\quad \left. + \sqrt{P_2(t - \Delta t)} \exp[i\varphi(t - \Delta t) + i\varphi_{p2} + i\theta_2] \right|^2, \end{aligned} \quad (5)$$

where P_1 and P_2 are given by Eq. (3) and the phase $\varphi(t)$ should be taken from the solution of Eq. (4). (The role of parameters p_1 and p_2 will be explained below.) It is taken into account in Eq. (5) that laser pulses acquire different phases when passing along different arms of the interferometer and the corresponding phase difference is $\Delta\theta = \theta_2 - \theta_1 = 2\Delta L n \omega_0 / c$, where n is the fiber refractive index and the factor 2 stands because the pulses pass the delay line twice in the Michelson interferometer. It should be noted that the second term in Eq. (5) does not contain the factor $\exp(i\omega_0\Delta t)$ that reflects the fact that the phase difference of the pulses does not depend on the accuracy of their overlap Δt , but is determined by the difference $\varphi_{p2} - \varphi_{p1}$ and by the interferometer delay line. Here the phases φ_{p1} and φ_{p2} are acquired by laser pulses during the time, when the gain switched laser is under threshold (in the amplified spontaneous emission (ASE) mode). We will assume below that phase correlations of the electromagnetic field are destroyed very quickly in the ASE mode due to contribution of phase uncorrelated spontaneous transitions, such that the overall phase difference $\Delta\Phi = \varphi_{p2} - \varphi_{p1} + \Delta\theta$ can be considered as an uncorrelated random variable. Moreover, we will assume further that φ_{p1} and φ_{p2} (and with them $\Delta\Phi$) exhibit normal distribution with the rms $\sigma_\varphi = 2\pi$ [9].

In a gain-switched laser, Δt introduced in Eq. (3) exhibits fluctuations, which are usually referred to as a time jitter. The main source of the jitter here are fluctuations of the pump current pulse front (the intrinsic jitter of pump current pulses) and fluctuations of its amplitude I_p (the peak-to-peak value of

the current modulation). (Under fluctuations, we understand here random variations of Δt and I_p from pulse to pulse.) The relation between the jitter and fluctuations of I_p is defined by fluctuations of the delay occurring between the application of the current pulse and the emission of light (the so-called turn-on delay [18], [19]). However, at high modulation frequencies (more than 1 GHz) the carrier number N does not have time to get well below threshold; therefore, fluctuations of I_p cannot provide significant fluctuations of the turn-on delay and thus does not contribute significantly to the time jitter. Therefore, the main contribution to the jitter at high modulation frequencies is given by the intrinsic jitter of pump current pulses. We will assume below that fluctuations of Δt due to jitter exhibit normal PDF; the rms of the jitter we will denote by $\sigma_{\Delta t}$.

Due to the relationship between the injection current and the shape of the optical signal, it is obvious that fluctuations of I_p will lead also to random changes in the output optical power $P(t)$. If the pump current fluctuations are relatively small, one can neglect the change in the pulse shape and assume that only the “area” under the pulse varies from pulse to pulse. This fact is taken into account in Eq. (5) by parameters p_1 and p_2 , each of which is a random variable with the mean value equal to $\bar{p}=1$ and with the PDF f_p defining the relationship between fluctuations of the injection current and $P(t)$. We assume that f_p has the form of a normal distribution with the rms of σ_p . It is important to note that although introduced random variables p_1 and p_2 have the same mean value and exhibit equivalent PDFs with the same rms value, they cannot be substituted by a single random variable p , since fluctuations of $P_1(t)$ and $P_2(t)$ are independent.

We now begin to consider the PDF of the random interference signal. In order to simplify further analysis, it makes sense to get rid of the time dependence in $S(t)$ considering instead the integral signal:

$$\tilde{S} = \frac{\int_{-T/2}^{T/2} S(t) dt}{\int_{-T/2}^{T/2} P_1(t) dt}, \quad (6)$$

where T is a time window cutting out a separate pulse from the pulse train (T corresponds here to the pulse repetition period), and normalization is performed with respect to the pulse exiting from the short arm of the interferometer. A further problem is then reduced to finding the PDF of the integral signal \tilde{S} , which we will denote by $f_{\tilde{S}}$.

In concern with integration of the signal according to Eq.

(6) it should be noted that such an approach may seem not similar to how such measurements are usually performed with fast detectors and oscilloscopes. In fact, a fast digital

oscilloscope with sufficiently high bandwidth (say, more than 30 GHz) will allow getting the result of the interference of chirped laser pulses even if they are shifted (i.e. delayed) relative to each other. So, it seems that if the detection is accomplished by sampling the interference signal within the pulse, the chirp will not affect the statistics of the recorded signal. However, it is not true for the case, when laser pulses are subject to significant jitter. In this case, the profile of the resulting pulse will be different for different pairs of interfering pulses, such that the pulse sampling in a certain point will anyway provide a range of values even if the phase difference between the pulses is always the same. This means that accumulating sampling points to measure PDF we will perform some kind of integration. Generally, selecting different points within the pulse to measure statistics of the interference signal, we could get various appearances of the PDF; therefore, to avoid ambiguity it seems to be more preferable to perform measurements integrating the whole pulse instead of sampling a single point. Therefore, the model based on the use of Eq. (6) is reasonable when one considers the interference of chirped laser pulses affected by jitter.

Finally, note that in a real experiment, the PDF of the interference signal is additionally “broadened” due to noises in the photodetector. The experimental signal should be therefore written as follows:

$$\tilde{S} \rightarrow \tilde{S} + \zeta, \quad (7)$$

where ζ is the noise signal, whose probability distribution is generally considered to be Gaussian.

We found the PDF of the integral signal with Monte-Carlo simulations using the following procedure. We set the time dependence of the pump current in the form of a train of rectangular pulses, $I(t) = I_b + I_p(t)$, where I_b is the bias current (the electric pulse width we denote by w – see Table I). With such $I(t)$, we solved numerically rate equations (4) and selected a pulse within the time window $[-T/2, T/2]$ (one pulse repetition period) far enough from $t=0$, such that the selected pulse was not affected by transients. Then for each set of random values Δt , φ_{p1} , φ_{p2} , p_1 , and p_2 we calculated $S(t)$ according to Eq. (5), assuming that $T_{01}T_{10} = T_{02}T_{20} = 0.25$ (an ideal coupler) and $a_1 = a_2 = 0$. (Note that to fit experimental data we use below $a_1 \neq a_2$.) At each iteration, we calculated the value of \tilde{S} according to Eq. (6). 10^5 iteration were found to be enough to get quite detailed statistics. Common laser and pump current parameters used for simulations are listed in Table I; the rest parameters varied depending on the simulation.

We will now consider three different models (see Fig. 2) to show the contribution of various effects. The first model (Fig. 2(a)) corresponds to the case of $I_b = 7$ mA, $I_p = 10$ mA, $\chi = 25$ W⁻¹, and $\alpha = 0$ (other parameters were taken from Table I). The photodetector noise was included according to Eq. (7) with rms $\sigma_{\zeta} = 0.05$. One can see that the

laser pulse in this case has a bell-type shape, which, with a good accuracy, can be represented by the Gaussian function. Since the linewidth enhancement factor was put to zero, the rate equation for the phase yields: $d\varphi/dt \equiv \Delta\omega = \omega - \omega_0 = 0$, i.e. the laser pulse is chirpless. One can easily find the integral signal \tilde{S} of the Gaussian chirpless pulse according to Eqs. (5) and (6):

$$\tilde{S} = s_1 + s_2 + 2\eta_{\Delta} \sqrt{s_1 s_2} \cos \Delta\Phi, \quad (8)$$

where s_1 and s_2 are normalized integral signals exiting from the short and long arms of the interferometer, respectively, and the visibility η_{Δ} is given by $\eta_{\Delta} = \exp(-\Delta t^2/8\delta^2)$, where δ is the rms width of the laser pulse. Normalized signals s_i are related to random variables p_i introduced above in the following way: $s_1 = p_1$ and $s_2 = rp_2$, where

$$r = \frac{(1-a_2)T_{02}T_{20}}{(1-a_1)T_{01}T_{10}}, \quad (9)$$

and therefore, the rms of their fluctuations is the same, i.e. $\sigma_s = \sigma_p$. According to the above assumption ($a_1 = a_2$), we have $r = 1$. One can see from Fig. 2(a) that the PDF exhibits noticeable asymmetry: the left maximum is higher and “thinner” than the right one. This feature is due to fluctuations of normalized amplitudes s_1 and s_2 and it becomes more pronounced when increasing the rms value of these fluctuations.

TABLE I
LASER AND PUMP CURRENT PARAMETERS, USED FOR SIMULATIONS IN FIGS. 2 AND 3. THE REST PARAMETERS VARIED DEPENDING ON THE SIMULATION.

Laser	Value	Pump current	Value
N_{th}	6.5×10^7	w	200 ps
N_0	5.0×10^7	$\omega_p/2\pi$	2.5 GHz
C_{sp}	10^{-5}	$\sigma_{\Delta t}$	10 ps
Γ	0.12	σ_p	0.05
ε	0.3		
τ_e	1.0 ns		
τ_{ph}	1.0 ps		

The picture is more complicated, if the Henry factor is non-zero. In this case, the time dependence of $\Delta\omega$ (the chirp) follows the time evolution of the carrier number $N(t)$ (see Eq. (4)), and $\Delta\omega = 0$ at $N = N_{th}$. In Fig. 2(b) we put $\alpha = 6$ without changing the bias current. One can see from the figure that $\Delta\omega(t)$ is approximately linear along the laser pulse profile (of course, it is not linear, when the contribution of spontaneous emission is not negligibly small). In fact, it is easy to find from Eq. (4) that the chirp of the Gaussian laser pulse is $\Delta\omega(t) = -\beta t$, if the spontaneous emission and the gain saturation are neglected (here, $\beta = \alpha/2\delta^2$). (If, however, $\chi \neq 0$, the time dependence of $\Delta\omega$ deviates from the straight

line.) The result of the interference differs now from the chirpless case; this is clearly manifested in a change of the PDF appearance shown in Fig. 2(b), where one can see the high peak in the center. This peak indicates an increase in the probability that the signal equals to $\tilde{S} = s_1 + s_2$, which is the evidence of interference worsening.

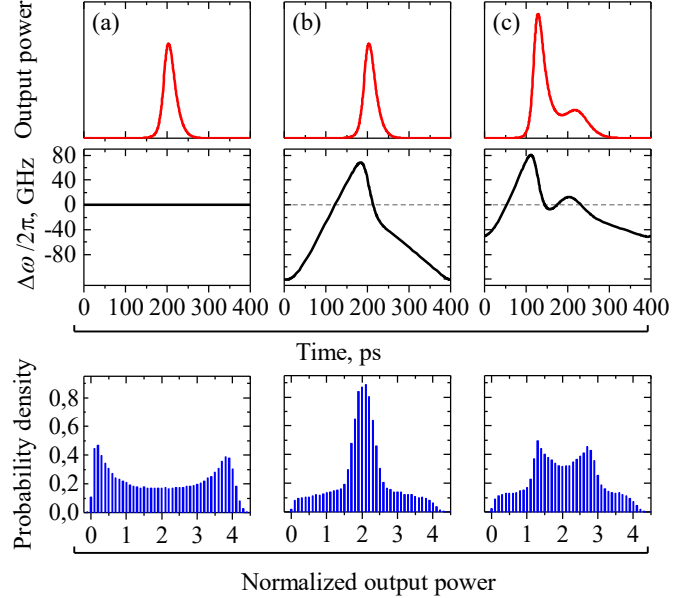


Fig. 2. The shape of the laser pulse (top), its chirp $\Delta\omega(t)$ (middle) and the PDF of the normalized interference signal (bottom) in different models: (a) chirpless ($\alpha=0$) bell-shaped laser pulse; (b) chirped ($\alpha=6$) bell-shaped laser pulse; (c) chirped ($\alpha=6$) laser pulse affected by relaxation spike. Simulation parameters are listed in Table I.

It should be noted that the difference between (a) and (b) cases in Fig. 2 is quantitative rather than qualitative in nature. In fact, the PDF of the interference signal given by Eq. (8) will also have a pronounced maximum at $\tilde{S} = s_1 + s_2$, if the rms of the jitter is quite large. So, the inclusion of the chirp increases the influence of the jitter. One can easily see this using Eq.

(4) for the linearly chirped Gaussian laser pulse. For such a pulse, the integral signal \tilde{S} is again defined by Eq. (8), but the visibility is given now by $\eta_{\Delta} = \exp[-(1+\alpha^2)\Delta t^2/8\delta^2]$, which indicates the increase of the jitter by a factor $\sqrt{1+\alpha^2}$.

It is important to note that in terms of visibility the interference does not deteriorate when adding chirp to the model. Indeed, although Δt and $\Delta\Phi$ in Eq. (8) have different values for different pairs of interfering pulses, there is a fairly high probability that the instant value of Δt will be zero and simultaneously $\Delta\Phi = \pi$ (which provides perfect destructive interference) or $\Delta\Phi = 0$ (which provides perfect constructive interference). However, the joint probability of these events decreases when increasing jitter, which leads to an increase in the central peak in the PDF of the integral signal \tilde{S} . Therefore, speaking about the deterioration of interference, we do not mean a decrease in visibility but the deviation of the signal PDF from that shown in fig. 2(a).

Finally, in Fig. 2(c) we consider a more general case, when the optical pulse is distorted by the first relaxation spike. For this, we increased the value of the bias current up to $I_b = 9$ mA (α was the same as in the previous simulation in Fig. 2(b)). One can see that due to the asymmetry of the output power $P(t)$, the chirp $\Delta\omega(t)$ has a quite complicated form. The PDF of the interference signal in Fig. 2(c) exhibits two pronounced maxima, which, in contrast to Fig. 2(a), do not correspond to an ideal constructive and destructive interference.

III. EXPERIMENT

We will now proceed to laser pulse interference measurements demonstrating obtained theoretical results. The optical scheme used in this work to observe interference of laser pulses is shown in Fig. 1. Unbalanced fiber optic Michelson interferometer was built using an optical circulator, a 50:50 single mode (SM) fiber coupler, SM fiber patch cable as a delay line, and two Faraday mirrors used to compensate the effects of polarization mode dispersion in SM fiber components. The length of the delay line ΔL was calculated using the following formula:

$$2\Delta L = \frac{2\pi N_p c}{\omega_p n_g}, \quad (10)$$

where c is the speed of light in vacuum, n_g is the group index, ω_p is the current modulation (angular) frequency corresponding to the pulse repetition rate, and N_p is the number of pulses emitted by the laser during the time when the given pulse travels the distance $2\Delta L$. In our case, ΔL was 128 cm, which at $\omega_p/2\pi = 2.5$ GHz provides $N_p = 32$, such that the first laser pulse interferes with the 33rd one, the second pulse interferes with the 34th one, etc.

The 1550 nm telecom distributed feedback (DFB) laser with 10 Gbps modulation bandwidth was driven by a commercial 11.3 Gbps low-power laser diode driver. Thermal stabilization of the laser diode was performed using Peltier thermoelectric cooler controlled by commercially available single-chip temperature controller. The waveform modulated at 2.5 GHz was generated by a phase-locked loops multiplying the input frequency from the 10 MHz reference oscillator. The peak-to-peak value of the modulation current I_p was estimated to be ~ 10 -12 mA. The laser threshold current I_{th} found from the light-current characteristics was estimated to be around 10 mA.

To detect the optical output, we used the home-built photodetector equipped by a p-i-n photodiode with 10 GHz bandwidth. The signal processing was performed using the Teledyne Lecroy digital oscilloscope (WaveMaster 808Zi-A) with 8 GHz bandwidth and temporal resolution of 25 ps. Optical spectra were acquired using Thorlabs optical spectrum analyzer (OSA 202) with a spectral resolution of 7.5 GHz.

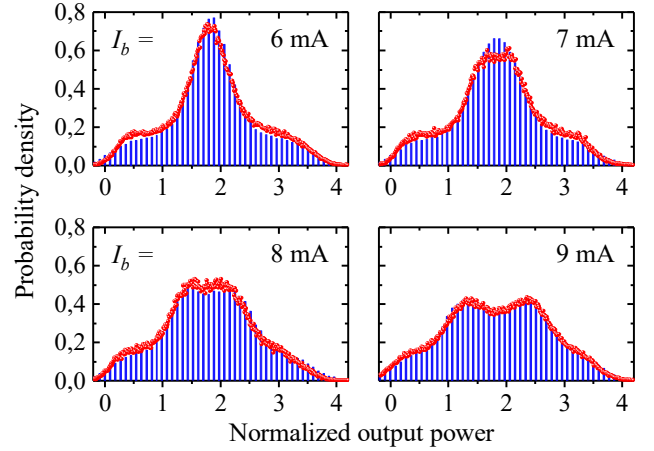


Fig. 3. Experimental PDFs of the interference signal at three different values of the bias current I_b (red circles) and corresponding Monte-Carlo simulations (histograms). The peak-to-peak value of the modulation current was ~ 10 mA in all cases.

Experimental PDFs of the interference signal at four different values of the bias current I_b are shown in Fig. 3 by red circles. Corresponding simulations are shown by blue histograms. For simulations, we used parameters from Table I. The rms of the normalized detector noise we put to $\sigma_\zeta = 0.25$, the gain compression factor was $\chi = 30 \text{ W}^{-1}$, and the peak-to-peak value of the pump current was $I_p = 11$ mA. As above, initial phases of laser pulses, φ_{p1} and φ_{p2} , were assumed to exhibit normal distribution with $\sigma_\varphi = 2\pi$. Finally, the interferometer arms were assumed to exhibit different losses (we put $a_1 = 0$ and $a_2 = 0.1$; these values were estimated experimentally). According to theoretical consideration, the contribution of relaxation oscillations at $I_b = 6$ mA is quite small; therefore, the corresponding PDF is similar to that shown in Fig. 2(b). The PDF at $I_b = 9$ mA is substantially different from that obtained at $I_b = 6$ mA due to the higher impact of relaxation oscillations. Intermediate PDFs in Fig. 3 are presented to demonstrate its evolution from lower to higher values of the bias current.

Obviously, the “chirp + jitter” effect can be reduced by either reducing jitter or chirp, or both. In our opinion, the simplest (and cheapest) solution is to use the bandpass filter to cut off a part of the laser spectrum associated with chirp. In the case of the Gaussian laser pulse with linear chirp, this approach would be more difficult, since it is necessary to cut off both the high- and low-frequency components of the spectrum. For the laser pulse affected by relaxation oscillations, the optical spectrum will have essential asymmetry, since only the rising edge of the laser pulse will be chirped significantly. One can see from Fig. 2(c) that when the relaxation spike occurs, the absolute value of $\Delta\omega$ decreases, which makes the falling edge of the pulse less chirped. Therefore, it is enough just to cut off the high-frequency part of the spectrum in this case.

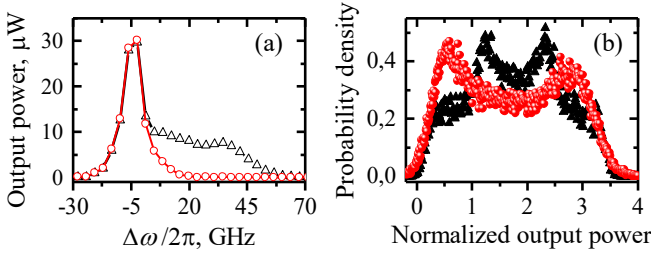


Fig. 4. (a) Experimental optical spectra at $I_b = 9$ mA without (empty triangles) and with (empty circles) DWDM filter. (b) Experimental PDFs of the interference signal at $I_b = 9$ mA without (filled triangles) and with (filled circles) DWDM filter.

To cut off the laser spectrum we used the telecom dense wavelength division multiplexing (DWDM) filter with 100 GHz bandwidth placed just after the laser output (see Fig. 1). The position of the laser spectrum on the frequency axis was adjusted by changing the laser temperature in such a way that the high-frequency shoulder was beyond the filter bandwidth. Experimental optical spectra at $I_b = 9$ mA without and with DWDM filter are shown in Fig. 4(a) by empty triangles and empty circles, respectively. The central frequency ω_0 corresponds to the “center of gravity” of the filtered spectrum at given temperature and is $\omega_0/2\pi = 193.63$ THz. One can see that the unfiltered spectrum has a broad high-frequency shoulder, which is related to the laser pulse chirp. Indeed, the corresponding PDF shown in Fig. 4(b) by filled triangles exhibits the specific shape caused by the interference of chirped non-Gaussian laser pulses (Fig. 2(c)). The PDF obtained with the DWDM filter (filled circles in Fig. 4(b)) exhibits two pronounced maxima corresponding to the constructive and destructive interference, as for the model shown in Fig. 2(a).

It should be noted here that the spectral filtering does not change the chirp itself – it only changes the intensity distribution of spectral components in the pulse. In fact, we observed a decrease in the intensity of the rising edge of the laser pulse after passing the optical filter, which is caused by the fact that its rising edge is chirped more significantly than the falling one. So, an optical filter improves spectral matching of the pulses improving thus their interference.

IV. CONCLUSIONS

We demonstrated that chirp, jitter and relaxation oscillations have a significant impact on probabilistic properties of the interference of laser pulses. It was shown that the relaxation spike makes the falling edge of the laser pulse less chirped and thus reduces the impact of the “chirp + jitter” effect on the appearance of the signal PDF. Moreover, the optical spectrum of the chirped pulse accompanied by relaxation oscillations exhibits significant asymmetry and can be easily cut off with a bandpass filter.

Note that in the context of a QRNG, the jitter should be considered as a source of a “classical” noise, since it is mainly caused by fluctuations of the pump current. Quantum noise originating in spontaneous emission and amplified via the

pulse interference is thus “contaminated” by the jitter. Therefore, the combined effect of the chirp and jitter is crucial when elaborating QRNG and must be minimized, e.g. with the use of the spectral filtering.

ACKNOWLEDGMENT

We are grateful to Aleksey Fedorov and Denis Sych for valuable comments.

REFERENCES

- [1] C. H. Bennett, G. Brassard, C. Crépeau, R. Jozsa, A. Peres and W. K. Wootters, “Teleporting an unknown quantum state via dual classical and Einstein-Podolsky-Rosen channels,” *Phys. Rev. Lett.*, vol. 70, pp. 1895-1899, 1993.
- [2] E. Knill, R. Laflamme and G. J. Milburn, “A scheme for efficient quantum computation with linear optics,” *Nature*, vol. 409, pp. 46-52, 2001.
- [3] S. L. Braunstein and S. Pirandola, “Side-Channel-Free Quantum Key Distribution,” *Phys. Rev. Lett.*, vol. 108, pp. 130502-1–130502-4, 2012.
- [4] H.-K. Lo, M. Curty and B. Qi, “Measurement-Device-Independent Quantum Key Distribution,” *Phys. Rev. Lett.*, vol. 108, pp. 130503-1–130503-5, 2012.
- [5] M. Jofre, M. Curty, F. Steinlechner, G. Anzolin, J. P. Torres, M. W. Mitchell and V. Pruneri, “True random numbers from amplified quantum vacuum,” *Opt. Express*, vol. 19, pp. 20665-20672, 2011.
- [6] C. Abellán, W. Amaya, M. Jofre, M. Curty, A. Acín, J. Capmany, V. Pruneri and M. W. Mitchell, “Ultra-fast quantum randomness generation by accelerated phase diffusion in a pulsed laser diode,” *Opt. Express*, vol. 22, pp. 1645-1654, 2014.
- [7] Z. L. Yuan, M. Lucamarini, J. F. Dynes, B. Fröhlich, A. Plews and A. J. Shields, “Robust random number generation using steady-state emission of gain-switched laser diodes,” *Appl. Phys. Lett.*, vol. 104, pp. 261112-1–261112-5, 2014.
- [8] D. G. Marangon, A. Plews, M. Lucamarini, J. F. Dynes, A. W. Sharpe, Z. Yuan and A. J. Shields, “Long-Term Test of a Fast and Compact Quantum Random Number Generator,” *J. Lightwave Technol.*, vol. 36, pp. 3778-3784, 2018.
- [9] R. Shakhovoy, D. Sych, V. Sharoglazova, A. Udaltsov, A. Fedorov and Y. Kurochkin, “Quantum noise extraction from the interference of laser pulses in optical quantum random number generator,” *Opt. Express*, vol. 28, pp. 6209-6224, 2020.
- [10] Z. Fang, H. Cai, G. Chen and R. Qu, *Single Frequency Semiconductor Lasers*. Singapore: Springer Nature, 2017.
- [11] E. H. Böttcher, K. Ketterer and D. Bimberg, “Turn-on delay time fluctuations in gain-switched AlGaAs/GaAs multiple-quantum-well lasers,” *J. Appl. Phys.*, vol. 63, pp. 2469-2471, 1988.
- [12] M. M. Choy, P. L. Liu, P. W. Shumate, T. P. Lee and S. Tsuji, “Measurements of dynamic photon fluctuations in a directly modulated 1.5-μm InGaAsP distributed feedback laser,” *Appl. Phys. Lett.*, vol. 47, pp. 448-450, 1985.
- [13] K. Petermann, *Laser Diode Modulation and Noise*. Dordrecht: Kluwer Academic Publishers, 1988.
- [14] G. H. M. v. Tartwijk and D. Lenstra, “Semiconductor lasers with optical injection and feedback,” *Quantum. Semicl. Opt.*, vol. 7, pp. 87-143, 1995.
- [15] G. P. Agrawal, “Effect of gain and index nonlinearities on single-mode dynamics in semiconductor lasers,” *IEEE J. Quantum. Elect.*, vol. 26, pp. 1901-1909, 1990.
- [16] G. P. Agrawal and N. K. Dutta, *Semiconductor lasers*. Dordrecht: Kluwer Academic Publishers, 1993.
- [17] C. Henry, “Theory of the linewidth of semiconductor lasers,” *IEEE J. Quantum. Elect.*, vol. 18, pp. 259-264, 1982.
- [18] K. Konnerth and C. Lanza, “Delay between current pulse and light emission of a gallium arsenide injection laser,” *Appl. Phys. Lett.*, vol. 4, pp. 120-121, 1964.
- [19] J. C. Dymont, J. E. Ripper and T. P. Lee, “Measurement and Interpretation of Long Spontaneous Lifetimes in Double Heterostructure Lasers,” *J. Appl. Phys.*, vol. 43, pp. 452-457, 1972.

Roman Shakhovoy received MSc degrees in nanotechnology from Southern Federal University, Russia, in 2012. In 2015, he received PhD at the University of Orléans, France. He is currently the Senior Researcher at

Russian Quantum Center and QRate. His main research interests are semiconductor laser dynamics and quantum random number generators.

Violetta Sharoglazova received the BSc degree in laser physics and technologies from National Research Nuclear University MEPhI, Moscow, Russia. She is currently pursuing the MSc degree in photonics and quantum materials with Skolkovo Institute of Science and Technology, Moscow, Russia. She works as junior researcher in Quantum Communication Group of the Russian Quantum Center. Her research interests include semiconductor laser dynamics and quantum random number generators.

Alexander Udaltsov received BSc and MSc degrees in electrical engineering from Novgorod State University in 2002 and 2004, respectively. Has 20 years' experience in the field of radars and telecommunications. Joined Quantum Communication Group of Russian Quantum Center in 2018 as a lead engineer. Main research focus is signal processing and quantum random number generation.

Alexander Duplinskiy received BSc and MSc degrees from Moscow Institute of Physics and Technology, PhD at Moscow Institute of Physics and Technology. He has been carrying out research on quantum key distribution for 5 years at Russian Quantum Center and QRate. Main research focus is quantum cryptography.

Vladimir Kurochkin received the Diploma degree in physics from the Novosibirsk State University, Russia, in 1976. In 1991, he received PhD degree from the Novosibirsk State University, Russia. He is currently the Principal Researcher at Russian Quantum Center and QRate. Currently, his main research focus is quantum cryptography.

Yury Kurochkin received MSc degree from Moscow Institute of Physics and Technology, PhD from Institute of Laser Physics, SB RAS, has 15 years' experience in quantum communications. He is currently Quantum Communication Group leader in the Russian Quantum Center and CTO of the QRate startup. His main research focus is applied quantum key distribution.